Journal Pre-proofs

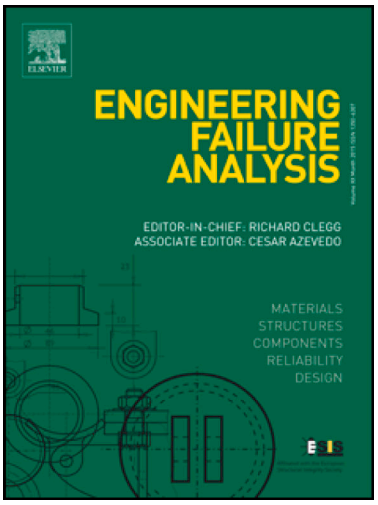

Manufacturing effects on fatigue strength

Moises Jimenez-Martinez

PII: S1350-6307(19)31226-9
DOI: https://doi.org/10.1016/j.engfailanal.2019.104339
Reference: EFA 104339

To appear in: *Engineering Failure Analysis*

Received Date: 19 August 2019
Revised Date: 6 November 2019
Accepted Date: 20 November 2019

Please cite this article as: Jimenez-Martinez, M., Manufacturing effects on fatigue strength, *Engineering Failure Analysis* (2019), doi: https://doi.org/10.1016/j.engfailanal.2019.104339

Manufacturing effects on fatigue strength

Moises Jimenez-Martinez moisesjimenezmartinez@gmail.com

Tecnológico de Monterrey, Escuela de Ingeniería y Ciencias

Abstract.

The fatigue strength of a component is affected by parameters such as geometry, applied loads and material. Although it is theoretically possible to have the same fatigue life in components from the same production lot, there is likely scatter in the measurements of fatigue. The scatter can influence the expected fatigue life, change the S-N curve for the component and adversely impact the stress amplitude axis. In this work, the effect of manufacturing on the fatigue life of a rear axle stabilizer is analysed. The evaluation of the residual stress that results from the manufacturing process suggested that durability was improved, as indicated by the rotation of the S-N curve around the axis, which represents the number of cycles. An optimization of the estimated S-N curve was proposed, it is based on the stresses generated on the manufacturing process, and the slope was increased to account for residual stress. A nonlinear finite element simulation was performed to find a factor that increases the expected fatigue life. The factor depends on the stress generated on the component, both with and without residual stress, and is computed using finite element results. The improvements in the fatigue life can be depicted by rotating the S-N curve and increasing its slope. The error in the fatigue life prediction using the estimated S-N curve was reduced by 22.92% using the factor based on the manufacturing process.

Keywords: Fatigue strength; manufacturing effect; S-N curve; nonlinear simulation; residual stresses.

1.-Introduction.

To prevent failures during a component's service life, it is necessary to evaluate the durability of the component under all the possible load conditions to guarantee the absence of failures. Mechanical components are subjected to complex service loadings and an accurate evaluation of durability is used as the basis for determining fatigue life under cyclic load conditions.

Durability is impacted by four main factors: loading, design, manufacturing and material selection (Jimenez, 2018). The integration of these factors impacts the component's fatigue strength (Berger et al, 2002).

Fatigue strength can be impacted by material selection and design. A design can have included tolerances associated with the manufacturing production goals, and scatter can occur due to variability among different lots of materials. Scatter can occur even if a component is produced from the same lot of material during the same production shift. In addition, another source of scatter comes from loads due to different driver profiles and driving conditions can modify the response to loads that are applied and transmitted by the chassis in an automobile, leading to substantial scatter (Robak and Lagoda, 2018). A fatigue test can be used to identify the most aggressive driver by studying components with the lowest mechanical properties. Failure likelihood is the probability of the failure when high loads are applied to the worst components (Roué et al., 2020).

The factors of design, material properties and loads are compared using the Damage rule to predict fatigue life. Quantifying cumulative fatigue damage due to several periods of applied stress is an old but not yet resolved problem (Jinescu, 2013; Schoenborn et al., 2016). The summation of the loads applied on the component during the periods of stress is also known as the time history or spectrum. The damage to the component is due to the cumulative summation of loads (Jinescu 2016). The Linear Damage Rule is still the most commonly used method to predict durability, due to its simplicity and accuracy. However, to further improve the life predictions using this rule, a correction factor can be applied that considers the sequence of the loads (Jimenez et al., 2015), as shown in equation 1.

$$\sum_{i}^{k} \frac{n_i}{N_i}(f) = W \quad (1)$$

where the amount of damage for each repetition (n_i) is evaluated for the number of repetitions tolerated (N_i) at the i load level and W is the total damage at failure.

Four main regions are typically considered in a Wöhler curve: the Extremely Low Cycle Fatigue (*ELCF*), Low Cycle Fatigue (*LCF*), High Cycle Fatigue (*HCF*) and Very High Cycle Fatigue (*VHCF*). High Cycle Fatigue is identified using the transition between *LCF* and *HCF*, defined as S_{1000}, and the behaviour in the limit of *HCF*, defined as S_{be}. The latter is modified to include other factors, such as load type (C_L), reliability (C_R), surface roughness (C_S) and a size factor (C_D). These factors shift the point S_{be} to $S_{e,R}$, thereby rotating the

curve in the *HCF* around S_{1000} and decreasing the slope. The weakest zone in a component is found at the surface (Pineau and Antolovich, 2016; Vayssette et al., 2019). Any modification of the component, such as shot penning, which induces localized plastic deformation, can improve the fatigue strength (Susmel et al.,2009). Residual compressive stresses and surface hardening can delay crack initiation and reduce crack propagation rates (Dalaei and Karlsson, 2012; Lee et al., 2017).

The turning process, when it is implemented as the final step in the manufacturing process, introduces residual tensile stresses on the surface; hence, it is detrimental to the fatigue life of a component. When induction, hardening and tempering are the last steps in a process, the residual stresses are minimal, and the fatigue life of the components is higher than for other common processes (Božić et al., 2018). The fatigue life of the tubes is largely dependent on the induced residual stresses that are generated during the manufacturing stage (Gerin et al., 2017). The manufacturing processes and their sequence of execution have a strong influence on the nature of the residual stress distribution (Kannan and Srinivasan, 2013). Shot penning improves the fatigue resistant properties of materials due to the formation of a hardened surface layer and the generation of compressive residual stress (Gu et al., 2019; Jinescu et al., 2017). The shot-peened surface is affected by the particle diameter and shot peening pressure. The amount of released compressive residual stress tends to increase with shot peening time (Kikuchi et al., 2016).

In this study, the fatigue in a stabilizer from a rear rigid axle was analysed. Rear axle is the support that reduce and transmit road forces with the car, its functions is link the road through wheels and chassis sub-assembly with the body car. Wheel´s position depends on the suspension linkage, the kinematic dimensions, and the compression or extension of the suspension. In lateral dynamics, it contributes to the stability of the lateral forces and nonsymetrical loads that are manage by the torsion bar. As other chassis parts this is a safety component, any failure on it could be result on a lack of stability on turns or overtake (Koh 2009).

Experimental results include surface transformation for a thermal treatment as well as sandblasting. The manufacturing process was evaluated to understand the impact on the prediction of fatigue life. Based on its effect, a factor was proposed to include extrusion process in fatigue life prediction, its effect is beneficial, improving fatigue performance.

2.- FINITE ELEMENT SIMULATION.

To predict the mechanical response, a Finite Element Analysis was performed on the axle. The material had the following properties: Young's modulus E=210,000 MPa, Poisson's ratio ν=0.3, and density ρ=7.8e-9 ton/mm^3. The stabilizer material was Steel 28Mn6 quenched and tempered (+QT). Table 1 depicts the material composition. The ultimate strength, σ_u, was 750 MPa, and the fracture elongation was 13%.

The software used for the pre-processor was Hypermesh, the solver used was Optistruct, and the post-processor used was HyperView. The rear axle was constructed using 123,458 first-order elements, 51,620 solid elements, 71,140 shell elements, and 698 rigid elements, as shown in figure 1. The nominal size of the elements was 3 mm, based on the convergence analysis shown in figure 2.

The critical load case for the stabilizer was torsion. To simulate torsion at the centre of the kinematic point in the wheel hub, a displacement (d_z), which was 180° out of phase between both sides, was applied. The kinematic point was fixed to the body of the car to limit the Degrees Of Freedom (DOF), except for the rotation around the y-axis, as shown in figure 3.

The stress results are shown in figure 4. Figure 4a shows the results for the axle, while figure 4b shows the isolation of the stabilizer. The maximum stress level predicted was 209.9 MPa.

2.1 Nonlinear Finite Element Simulation.

To simulate an accelerated stabilizer test, the bar was isolated, and direct torsion was applied to increase the frequency of the test and to eliminate the physical constraints associated with the axle assembly. The amplitude of the rotation was calculated using geometric properties. For a displacement, d_z, of 30 mm, an angle of 7.7° was generated in the bar. For a displacement of 40 mm, the angle was 9°. For a 50 mm displacement, an angle of 12.9° was generated.

A finite element model was created with 33,595 first-order hexahedral elements. The size of the elements was 3 mm. The spatial constraints were limited to the six Degrees of Freedom in the centre of the tube. The characteristic property of the extrusion was the mass of the tooling, 0.5 tons, and it impacted the velocity. Although extrusion processes are typically performed in two steps – the first step is performed on one side, then the part is rotated, and the operation is performed on the other side – the simulation was simplified to perform the operation on both sides simultaneously. Normal and tangential contacts were found in the area of extrusion between the tooling and the internal surface of the tube. A dynamic coefficient of friction of 0.15 was applied, as shown in figure 6. The same contact was applied to both sides.

Figure 6 shows the movement of the tooling. The initial position had a distance of 50 mm between them (figure 6a); then, the tool moved to the edge of the tube (figure 6b). The tube then underwent plastic deformation (figure 6c) and had a modified shape (figure 6d). In the final image, the stress distribution can be seen following the extrusion process.

To evaluate the effect of velocity on the residual stress distribution, different velocities were simulated. Figure 7 shows the strain energy history for the velocities evaluated. The results from figure 7 suggest that the velocity does not affect the plastic behaviour during the process. The results also suggest that the maximum energy value was increased, which reduced the velocity from 2000 mm/sec to 1500 mm/sec. Reducing the velocity to 1000 mm/sec had a tendency to reduce it; however, at 500 mm/sec, it increased to a maximum value. When the maximum value of 2000 mm/sec was evaluated with a lower velocity, a correlation of 98.1% of the peak value was obtained.

The deformed mesh model from the nonlinear simulation was imported to a new static model. The boundary conditions, which were applied on one side, restricted the movement to 6 DOF. On the other side, a rotation of 7.7° was applied to simulate pure torsion. The maximum von Mises stress was 207 MPa, and the shear contact force was 119.7 MPa, as predicted from the stress calculations.

To include the effects of the manufacturing process on the stress generated in the static load case, it is important to include the residual stress from the nonlinear simulation. For the simulation of this case, instead

of assuming that the model was free from residual stress, the residual stress shown in figure 6 was the initial stress state of the model. The rotation applied was 7.7°, which was similar to when the model was free of residual stresses. The results are shown in figure 8. The von Mises stress was 177.6 MPa, and the shear stress was 107.4 MPa. For an angle of 9°, the von Mises stress was 239.4 MPa. With the initial stress values from the extrusion simulations, the von Mises stress was 203.3 MPa. For an angle of 12.9°, the von Mises stress was 343.3 MPa. With the initial stress values from the extrusion simulations, the von Mises stress was 280.058 MPa. The stress loads were reduced by factors of 1.15, 1.17 and 1.22, with an average of 1.18 times the stress reduction.

3.- EXPERIMENTAL ANALYSIS.

The setup was built using a rotary actuator with a maximum moment of 2260 Nm, a dynamic rotation of 90°, and static rotation of 100°. The working pressure was 210 bar, and the control was accomplished using a Flextest GT servocontroller. The stabilizer was aligned using a laser to guarantee pure torsion. Figure 9a shows the alignment on the top surface, and figure 9b shows the alignment with the horizontal position. For both cases, it was verified that the centre position on the device was fixed to ensure alignment of the tested specimen to the centre of the rotational actuator.

The simulated results for the prediction of the failure area are shown in figure 10a and are compared with experimental results in figure 10b. Failure is found it near of the minimum extrusion diameter. The fissure propagation is shown in figure 11.

3.1.-Estimated S-N curve.

In a previous study by the author, a relationship that estimated the fatigue strength at 1000 cycles (S_{1000}) for nodular cast iron was proposed (Jimenez et al., 2014). In this work, in the first part of the analysis, the same relationship will be used to predict the expected fatigue life in the steel stabilizer bar, and is proposed a relationship to improve fatigue life prediction. During the fatigue assessment, it was necessary to consider different factors that reduced the endurance limit. These factors are expressed in equation 2.

$$S_{e,R} = 0.4 \times S_u \times C_{(L,S,D,R)} \quad (2)$$

where C_L is the load factor (0.58 for bending); C_S is the surface factor; C_D is the size; and C_R is the reliability factor. It is assumed that the estimated S-N curve had a 50 % probability of failure, for a midrange

fatigue curve, such that C_R=1 (Kepka and Kepka Jr., 2018; Lee et al., 2005). The surface finish was polished; thus, C_S=1. The size coefficient in a specimen with a diameter below 8 mm is 1; otherwise it is defined by equation 3 as follows:

$$C_D = 1.189 \times d^{-0.097} \quad (3)$$

The relationship proposed for a reliability of 50 % is defined to estimate $S_{1000\text{-}2}$ as shown in equation 4 (Jimenez et al., 2014):

$$S_{1000-2} = S_u - \frac{1}{2} S_u \times \ln \frac{1}{K} \quad (4)$$

The factor K depends on the type of loading; for bending, K=0.9, for an axial load, K=0.75, and, for torsion, K=0.63 (Lee et al., 2005)

The ultimate strength was 750 MPa, and the specimen had a radius of 20 mm. From equation 3, we obtained C_D=0.831 and a bending load of C_L=0.58. From equations 2, the value $S_{e,R}$=115.43 MPa was obtained. From equation 4, we obtained $S_{1000\text{-}2}$=616.8 MPa .

The N at $S_{e,R}$ could likely be modified in order to take into account improvements in fatigue life prediction. Any improvement to the fatigue life is expressed as a translation of $N_{Se,R}$ on the cycle (N) axis. The translation generates a rotation and increases the slope, as shown in figure 12.

The factor that multiplies the $N_{Se,R}$ is thought to depend on the stress reductions due to the manufacturing process. The factor is the ratio of the stress without residual stress to the residual stress at load level i. From the nonlinear simulations, the average of this value was 1.1856. A general value S_μ is included:

$$N_{Se,R(\text{mod})} = N_{Se,R} \times S_\mu \quad (5)$$

To evaluate the proposed S-N curve, we compared the experimental results with the simulated S-N curve. For a given S-N data point (S_1,N_1), the inverse slope k can be used to determine the number of equivalent damage cycles (N_2) for the stress amplitude (S_2) as follows:

$$N_2 = N_1\left(\frac{S_1}{S_2}\right)^k \quad (6)$$

The slopes for both the estimated curves were found using equations 7 and 8:

$$b = \frac{\log S_{1000} - \log S_{e,R}}{\log 1x10^3 - \log 5x10^8} \quad (7)$$

$$k = -\frac{1}{b} \quad (8)$$

The results were evaluated using the S-N predicted fatigue life. The values were calculated using equations 6, 7 and 8 and were compared with the experimental results.

From equation 5, the adjusted value $N_{Se,R(mod)}$ was calculated, and failure was predicted at 1,185,600 cycles. Based on this value in equation 7, b_{mod}=-0.239, and the slope in equation 8 indicated that k_{mod}=4.183.

4.-RESULTS AND DISCUSSION.

A summary of the fatigue life predictions, calculated using equation 4, are summarized in table 2. Table 2 shows the amplitude, expressed in degrees, the stress generated and the expected life, which were predicted using the Jimenez and the proposed relationships. Table 3 shows the predicted differences between the expected life and the median (μ) of the experimental results.

The failure values were evaluated, and the original design was shown to have an average prediction of 42.43%. Using Jimenez's relationship without adjusting $N_{Se,R}$ and without considering the residual stresses from the extrusion, as well as considering both factors ($N_{Se,R(mod)}$ and residual stresses), the predicted error was reduced from 57.67% to 20.70%.

For the results obtained following thermal treatment, the error predicted using Jimenez's relationship had an average of 17.01% and 5.91%. The averages considered the application of the thermal treatment before and after the extrusion; using the described corrections, the predictions were improved to 39.75% and 12.82%, respectively.

As was expected, all the improvements on the surface components led to improved fatigue strength. The highest improvement occurred with sand blasting due to the compressive stress on the surface. The results were 1.55 times greater than the predicted fatigue life at 7.7° and 31.42 times. However, it is not possible to define a factor to increase the slope and improve fatigue life predictions since there are no failure results.

5.-CONCLUSIONS.

The relationship proposed by the author, which was originally developed for nodular cast iron, was modified to estimate the S-N curve for steel under torsion conditions and to consider the manufacturing effects $N_{Se,R(mod)}$. In this case, the residual stress generated by extrusion was reduced an average of 1.1856 times. The factor used in the relationship proposed is defined using finite element analysis with and without residual stress from the manufacturing process. The factor can be used to increase the number of expected cycles at the $S_{e,R}$ load level and the rotation of the S-N curve. With the increase in the slope, the error in the prediction was reduced to 36.95%.

For the cases where more than one result was obtained at each load level, a standard deviation was evaluated, and a maximum value of 0.22 was calculated. The value was lower than the maximum value tolerated (0.3) for a uniaxial test and adds validity to the test results (Jimenez, 2017). The results suspended without failure were not used to calculate life predictions and were only evaluated to identify qualitative improvements.

Fatigue failure of rear axle torsion bar were reported by ten results without any bar modification, five components with thermal treatment to the material prior extrusion, three components with thermal treatment after extrusion and two bars with sandblasting suspended without failure.

Thermal treatments have beneficial effects on fatigue life, and the predictions were improved by 22.73% and 6.91%. However, for thermal treatments done before and after extrusion and that included residual stress as well as the correction proposed in $N_{Se,R(mod)}$, it was not possible to predict fatigue using a factor. Residual stress in the microstructure due to the manufacturing process was evaluated; however, changes in the microstructure were not considered. Changes were analysed using the experimental results from sand blasting due to its compressive residual stress on the surface, and sand blasting was identified as the best solution. However, it was not possible to define a proposed solution since the tests were suspended without failure.

REFERENCES.

[1] M. Jimenez, Accelerated Fatigue Test in Mechanical Components. In: Pranav H. Darji and Veera P. Darji Contact and Fracture Mechanics, IntechOpen, 2018, pp. 253-273. DOI: 10.5772/intechopen.72640

[2] C. Berger, K.-G. Eulitz, P. Heuler, K.-L. Kotte, H. Naundorf, W. Schuetz, C.M. Sonsino, A Wimmmer, H. Zenner, Betriebsfestigkeit in Germany- an overview, Int. J. Fatigue 24 (2002) 603-625. https://doi.org/10.1016/S0142-1123(01)00180-3

[3] G. Robak, T. Lagoda, Variability of fatigue parameters under uniaxial loading in the function of the number of cycles to failure, Int. J. Fatigue 113 (2018) 246-252. https://doi.org/10.1016/j.ijfatigue.2018.04.003

[4] V. Roué, C. Doudard, S. Calloch, Q. P. d´Andrebo, F. Corpace, C. Guévenoux, Simulation-based investigation of the reuse of unbroken specimens in a staircase procedure: Accuracy of the determination of fatigue properties, Int. J. Fatigue 131 (2020) 105288. https://doi.org/10.1016/j.ijfatigue.2019.105288

[5] V. V. Jinescu, Critical energy approach for the fatigue life calculation under blocks with different normal stresses amplitudes, Int. J. Mech. Sci. 67 (2013) 78-88. https://doi.org/10.1016/j.ijmecsci.2012.12.009

[6] S. Schoenborn, H. Kaufmann, C.M. Sonsino, R. Heim, Variable amplitude fatigue of high-strength cast iron alloys for automotive applications, Int. J. Fatigue 91 (2016) 445-458. https://doi.org/10.1016/j.ijfatigue.2016.01.006

[7] V.V. Jinescu, Fatigue life prediction for simultaneous cyclic loading with blocks of normal stresses and shear stresses, Journal of Engineering Sciences and Innovation 1 (2016), 1-16.

[8] M. Jimenez, J. Martinez, U. Figueroa, Load sequence analysis in fatigue life prediction, Trans. Can. Soc. Mech. Eng. 39 (2015) 819-828. https://doi.org/10.1139/tcsme-2015-0065

[9] A. Pineau, S.D. Antolovich, Probabilistic approaches to fatigue with special emphasis on initiation from inclusions, Int. J. Fatigue 93 (2016) 422-434. https://doi.org/10.1016/j.ijfatigue.2016.09.002

[10] B. Vayssette, N. Saintier, C. Brugger, M.E. May, E. Pessard, Numerical modelling of surface roughness effect on the fatigue behavior of Ti-6Al-4V obtained by additive manufacturing, Int. J. Fatigue 123 (2019) 180-195. https://doi.org/10.1016/j.ijfatigue.2019.02.014

[11] L. Susmel, Three different ways of using the Modified Wöhler Curve Method to perform the multiaxial fatigue assessment of steel and aluminium welded joints, Eng. Fail. Anal. 16 (2009) 1074-1089. https://doi.org/10.1016/j.engfailanal.2008.05.016

[12] K. Dalaei, B. Karlsson, Influence of shot peening on fatigue durability of normalized steel subjected to variable amplitude loading, Int. J. Fatigue 38 (2012) 75-83. https://doi.org/10.1016/j.ijfatigue.2011.11.011

[13] K.T. Lee, C.S. Park, H.Y. Kim, Fatigue and buckling analysis of automotive components considering forming and welding effects, Int. J. Automot. Technol, 18 (2017) 97-102.

[14] Ž. Božić, S. Schmauder, H. Wolf, The effect of residual stresses on fatigue crack propagation in welded stiffened panels, Eng. Fail. Anal. 84 (2018) 346-357. https://doi.org/10.1016/j.engfailanal.2017.09.001

[15] B. Gerin, E. Pessard, F. Morel, C. Verdu, A. Mary, Beneficial effect of prestrain due to cold extrusion on the multiaxial fatigue strength of a 27MnCr5 steel, Int. J. Fatigue 92 (2016) 345-359. https://doi.org/10.1016/j.ijfatigue.2016.07.012

[16] S. Kannan, S.M. Srinivasan, Influence of manufacturing processes and their sequence of execution on fatigue life of axle house tubes in automobiles, Eng. Fail. Anal, 34 (2013) 79-92. https://doi.org/10.1016/j.engfailanal.2013.07.013

[17] C. Gu, J. Lian, Y. Bao, S. Münstermann, Microstructure-based fatigue modelling with residual stresses: Prediction of the microcrack initiation around inclusions, Mater. Sci. Eng., A 751 (2019) 133-141. https://doi.org/10.1016/j.msea.2019.02.058

[18] V.V. Jinescu, V.-N. Nicolof, A.Chelu, S.-E. M., Calculation of the local critical state taking into account the deterioration and the residual stresses, Journal of Engineering Science and Innovation 2(2017) 9-21.

[19] S. Kikuchi, Y. Nakamura, K. Nambo, M. Ando, Effect of shot peening using ultra-fine particles on fatigue properties of 5056 aluminum alloy under rotating bending, Mater. Sci. Eng., A, 652(2016) 279-286. https://doi.org/10.1016/j.msea.2015.11.076

[20] S.K. Koh, Fatigue analysis of an automotive steering link, Eng. Fail. Anal. 16 (2009) 914-922. https://doi.org/10.1016/j.engfailanal.2008.08.014

[21] M. Jimenez, J. Martinez, U. Figueroa, L. Altamirano, Estimated S-N curve for nodular cast iron: A steering knuckle case study, Int. J. Automot. Technol. 15 (2014)1197-1204. https://doi.org/10.1007/s12239-014-0125-4

[22] M. Kepka, M. Kepka Jr, Deterministic and probabilistic fatigue life calculations of a damaged welded joint in the construction of the trolleybus rear axle, Eng. Fail. Anal. 93 (2018) 257-267. https://doi.org/10.1016/j.engfailanal.2018.07.015

[23] Y.L. Lee, J. Pan, R.B. Hathaway, M.E. Barkey, (2005). Fatigue Testing and Analysis. Elsevier Buiterworth Heinemann, 1. p130.

[24] M. Jimenez, Durability tests: Statistical analysis for variable amplitude loads, Trans. Can. Soc. Mech. Eng. 41 (2017) 910-921. https://doi.org/10.1139/tcsme-2017-520

Fig. 1. Finite Element model for the rear axle.

Fig. 2. Convergence Analysis

Fig. 3. Spatial constraints and Boundary conditions.

Fig. 4. Stress results in the rear axle, (a) isometric view, (b) bottom view.

Fig. 5. Finite element model boundary conditions.

Fig. 6. Finite element simulation of extrusion at (a) 0 sec, (b) 0.0787 sec, (c) 0.1476 sec and (d) 0.225 sec.

Fig. 7. Strain Energy history.

Fig. 8. Results depicting torsion stress with residual stress, (a) von Mises stress and (b) shear stress.

Fig. 9. Durability test stand for a rear axle stabilizer, (a) frontal view, (b) lateral view.

Fig. 10. Failure (a) predicted using FEA and (b) the experimental results.

Fig. 11. Fissure propagation.

Fig. 12. Schematic of S-N curve rotation.

Fig. 13. S-N curve of the rear axle stabilizer.

Table 1. Nominal composition in % wt. 28Mn6 +QT, according to DIN EN 10083

C	Si	Mn	Mn	P	S	Cr	Mo	Ni	Cr+Mo+Ni
0.25-0.32	<0.40	1.3-1.65	0.10	<0.035	>0.035	<0.40	<0.10	0.40	<0.63

Table 2. Fatigue life prediction.

Angle (°)	Stress (Mpa)	$\mu_{Jimenez}$ (Cycles)
7.7	207.3	91,602
9.0	242.2	48,530
12.9	347.2	11,155

Table 3. Experimental results and fatigue life prediction.

Specimen characteristics	Amplitude	Experimental results			Prediction Jimenez		Prediction $N_{Se,R(mod)}$	
		Cycles	S_{log}	μ	cycles	%	cycles	%
Original design	7.7	392,440	0.21	315,402	91,602	29.04	172,221	54.60
	7.7	487,449						
	7.7	194,251						
	7.7	187,468						
	9	86,822	0.05	93,062	48,530	52.15	99,186	106.58
	9	108,752						
	9	83,090						
	9	84,441						
	9	102,207						
	12.9	24,349	-	24,349	11,155	45.81	26,814	110.12
Thermal treatment to the material prior extrusion	7.7	3,425,000	No failure					
	7.7	2,654,228						
	9	746,955	-	746,955	48,530	6.50	99,186	13.28
	12.9	26,382	0.22	40,515	11,155	27.53	26,814	
	12.9	54,648						66.18
Sand blasting	7.7	487,449	No failure					
	9	2,924,100						
Thermal treatment after extrusion	7.7	1,952,440	-	1,952,440	91,602	4.69	172,221	8.82
	9	1,014,880	-	1,014,880	48,530	4.78	99,186	9.77
	12.9	134,975	-	134,975	11155	8.26	26,814	19.87